Efficient degradation of sulfamethazine in simulated and real wastewater at slightly basic pH values using Co-SAM-SCS /H_2O_2 Fenton-like system

Min Cheng [a,b], Guangming Zeng [a,b,*], Danlian Huang [a,b,*], Cui Lai [a,b], Yang Liu [a,b], Chen Zhang [a,b], Jia Wan [a,b], Liang Hu [a,b], Chengyun Zhou [a,b], Weiping Xiong [a,b]

a. College of Environmental Science and Engineering, Hunan University, Changsha, Hunan 410082, China

b. Key Laboratory of Environmental Biology and Pollution Control (Hunan University), Ministry of Education, Changsha, Hunan 410082, China

∗ Corresponding author at: College of Environmental Science and Engineering, Hunan University, Changsha, Hunan 410082, China.

Tel.: +86–731– 88822754; fax: +86–731–88823701.

E-mail address: zgming@hnu.edu.cn (G.M. Zeng), huangdanlian@hnu.edu.cn (D.L. Huang).

Abstract

The presence of antibiotics in aquatic environments has attracted global concern. Fenton process is an attractive yet challenging method for antibiotics degradation, especially when such a reaction can be conducted at neutral pH values. In this study, a novel composite Fe/Co catalyst was synthesized via the modification of steel converter slag (SCS) by salicylic acid–methanol (SAM) and cobalt nitrate ($Co(NO_3)_2$). The catalysts were characterized by N_2-Brunauer–Emmett–Teller (BET), X-ray diffraction (XRD), Fourier transform infrared (FT-IR), X-ray photoelectron spectroscopy (XPS), scanning electron microscopy (SEM) and energy dispersive X-ray spectroscopy (EDS). The results indicated that the Co-SAM-SCS/H_2O_2 Fenton-like system was very effective for sulfamethazine (SMZ) degradation at a wide pH range. At initial pH of 7.0, the degradation rate of SMZ in Co-SAM-SCS/H_2O_2 system was 2.48, 3.20, 6.18, and 16.21 times of that in Fe-SAM-SCS/H_2O_2, SAM-SCS/H_2O_2, $Co(NO_3)_2$/H_2O_2 and SCS/H_2O_2 system, respectively. The preliminary analysis suggested that high surface area of Co-SAM-SCS sample and synergistic effect between introduced Co and SAM-SCS are responsible for the efficient catalytic activity. During the degradation, three main intermediates were identified by high performance liquid chromatography–mass spectrometry (HPLC–MS) analysis. Based on this, a possible degradation pathway was proposed. The SEM images, XRD patterns and XPS spectra before and after the reactions demonstrate that the crystal and chemical structure of Co-SAM-SCS after five cycles are almost unchanged. Besides, the Co-SAM-SCS presented low iron and

cobalt leaching (0.17 mg/L and 2.36 mg/L, respectively). The studied Fenton-like process also showed high degradation of SMZ in river water and municipal wastewater. The progress will bring valuable insights to develop high-performance heterogeneous Fenton-like catalysts for environmental remediation.

Keywords: Fenton-like; Sulfamethazine; Steel converter slag; Cobalt; Degradation.

1. Introduction

Antibiotics have been excessively abused in veterinary and human medicine. As emerging contaminants, they have drawn increasing attention in recent years owing to their potential adverse effects on human health and aquatic ecology (Cheng et al. 2016c, Zeng et al. 2013a). Due to their antibacterial and polarity nature, conventional waste-water treatment plants (WWTPs) can only partially remove antibiotics, demonstrating the potential for these compounds to be consistently presented in effluents (Lai et al. 2016, Li et al. 2017, Yang et al. 2010). As a result, antibiotics have been repeatedly detected in surface water and sediment (Cheng et al. 2018b, Guo et al. 2017, Huang et al. 2016, Liu et al. 2017, Zhang et al. 2016). Thus, an effective elimination of these compounds from the environment is important and necessary.

Advanced oxidation processes (AOPs) are promising techniques for the disposal of toxic and persistent organic pollutants in wastewaters (Cheng et al. 2017b, Huang et al. 2017, Yang et al. 2017, Yang et al. 2016). Among these techniques, Fenton process, based on the generation of highly reactive hydroxyl radicals (HO•), has received particular attention (Cheng et al. 2016b). The Fenton process holds many advantages, including high degradation efficiency, mild reaction conditions and

simple operation (Cheng et al. 2016a). However, Fenton process also suffers from some drawbacks, such as, (1) it requires strict pH regulation (pH 2–4) (Liu et al. 2016), (2) it requires the post-treatment of the dissolved iron ions and sludge (Guo et al. 2014), and (3) it may cause secondary pollution of acids (Burbano et al. 2005), which make this technique complex and uneconomical.

In order to overcome these drawbacks, Fenton-like processes using heterogeneous catalysts containing iron materials have been developed (Navalon et al. 2010). In recent years, hematite (α-Fe_2O_3), maghemite (γ-Fe_2O_3), magnetite (Fe_3O_4), pyrite (FeS_2) and goethite (α-FeOOH) have been applied as heterogeneous Fenton-like catalysts for the degradation of many organic contaminants over a wider pH range. Steel converter slag (SCS), a final waste material of the steel making process, has high potential to be used in the Fenton-like process as heterogeneous catalyst owing to its abundance of iron oxides (FeO and Fe_2O_3) (Yi et al. 2012). On the other hand, SCS also contains calcium minerals, which can negatively impact the performance of Fenton-like process. It was reported that after adding SCS into the system, solution pH could be rapidly increased from 6.4 to 10, due to the dissolution of calcium minerals (Cheng et al. 2018a; Cheng et al. 2017a). Under this condition, the Fenton/Fenton-like reaction would be inefficient. In our previous study, salicylic acid–methanol (SAM) solution was used to dissolve calcium silicate minerals in SCS and successfully improved the catalytic property of SCS (Cheng et al. 2017a). However, like other iron based heterogeneous Fenton-like processes, the degradation was preferentially operated at acidic solutions (pH <3) (Fan et al. 2009, Ozcan et al.

78 2017, Shen et al. 2017, Tang et al. 2008). Such a requirement of acidic environment,
79 however, limited the industrial application of the technology because the pollutant
80 solutions always have neutral or slightly basic pH values (Fan et al. 2008, Shen et al.
81 2017, Zeng et al. 2013b).

82 Previous studies have shown cobalt based Fenton/Fenton-like process can be
83 operated in neutral pH condition (Bokare and Choi 2014). On the one hand, the
84 homogeneous Co^{2+}/H_2O_2 system was found able to completely decompose the dye
85 pollutant without the control of pH (Ling et al. 2010). On the other hand, the
86 degradation of organic pollutants by heterogeneous Co catalysts was also studied in
87 the presence of H_2O_2. In one study, Co^{2+} loaded periodic mesoporous aluminum
88 phosphate was utilized as heterogeneous catalyst for the degradation of phenol
89 (Mahamallik and Pal 2016). In a more recent work, Co^{2+} adsorbed alumina was
90 applied as heterogeneous catalyst to decompose methylene blue and methyl orange
91 (Mahamallik and Pal 2017). In both cases, Co-based heterogeneous catalysts can
92 effectively degrade the pollutants at neutral or even basic pH.

93 Inspired by the above idea, in this study, we used Co^{2+} to further improve the
94 catalytic property of SCS in order to deal with the real wastewater, which always has
95 neutral or slightly basic pH values. The sulfamethazine (SMZ), one of the most
96 commonly used antibiotics, was selected as model antibiotics contaminant because of
97 its adverse effects on living being and frequently occurrence in natural water
98 environment (Sopaj et al. 2016). In recent years, chemical oxidation methods,
99 especially the AOPs, have been used for degradation of SMZ, including Fenton

reaction based processes (Wan et al. 2016, Wan and Wang 2017, Wang et al. 2017, Zhou et al. 2014, Zhou et al. 2013), photo-catalysis (Babić et al. 2015, Yap et al. 2012), gamma irradiation (Liu et al. 2014, Liu and Wang 2013), ozonation (Bai et al. 2016, Garoma et al. 2010) and dielectric barrier discharge plasma (Kim et al. 2013). According to the literature, Fenton reaction based processes have been most widely used for the degradation of SMZ mainly due to their low cost and high efficiency. The other methods may either suffer from high energy consumption or low efficiency. Many works have demonstrated the degradation of SMZ by Fenton reaction based processes; however, most of them were conducted at acidic condition (Wan and Wang 2017, Wang et al. 2017, Zhou et al. 2014, Zhou et al. 2013). Besides, few studies have considered the degradation pathways of SMZ in the system.

The main objectives of this work were to (1) produce a new heterogeneous Fenton-like catalyst and elucidate its morphology evolution process; (2) study the degradation performance of SMZ at neutral pH values in this Fenton-like system and investigate affecting experimental parameters; (3) clarify the Fenton-like reaction mechanism and reveal the promotional role of Co^{2+} in the Fenton-like process; and (4) examine the degradation intermediates of SMZ and propose the possible degradation pathways.

2. Experimental section

2.1. Reagents and materials

The SCS was provided by Valin Iron and Steel Corp (VISTC), Xiangtan, China.

121 The SCS is mainly composed of CaO, SiO_2, FeO, Fe_2O_3, MgO, MnO, Al_2O_3, P_2O_5
122 and TiO_2 (Table S1). The raw SCS was grinded with a planetary ball mill (YXQM-4L,
123 MITR, China) and sieved with a 0.05 mm mesh sieve to remove the large particles.
124 Sulfamethazine ($C_{14}H_{20}ClNO_2$, standard grade) was obtained from Sigma-Aldrich
125 (Missouri, USA). Cobalt nitrate hexahydrous ($Co(NO_3)_2 \cdot 6H_2O$, analytical grade),
126 methanol (chromatographic grade), salicylic acid ($C_7H_6O_3$, analytical grade) and
127 hydrogen peroxide (H_2O_2, 30% in water) were obtained from Beijing Sinopharm
128 Chemical Reagent Corp (China). Ultrapure water (18.3 $M\Omega \cdot cm^{-1}$) was used in all the
129 batch experiments.

130 *2.2. Preparation of SAM-modified SCS*

131 The preparation of SAM-modified SCS (SAM-SCS) was reported in a previously
132 work (Cheng et al. 2017a). Briefly, 50 g of the dried SCS powder was added in 100
133 mL SAM solution (50 g/L) and stirred at 200 rpm for 4 h at 25 ºC. The mixture was
134 then filtered with the suction filter machine using a 0.45 μm filter membrane. The
135 filtration residue was washed repeatedly with ultrapure water and then dried at 105 ºC
136 for 24 h.

137 *2.3. Preparation of Co-SAM-SCS*

138 Co^{2+} was introduced to the surface of SAM-SCS by a simple adsorption process.
139 At first, 1 g of prepared SAM-SCS was dispersed in a glass beaker containing 50 mL
140 of ultrapure water. The beaker was placed in a constant temperature (25 ºC) ultrasonic
141 bath to obtain homogeneous SAM-SCS dispersion. After 30 min, 2 mL of $Co(NO_3)_2$

142 solution (0.2 M) was equally and slowly added to the beaker and maintained for
143 another 0.5 h ultrasonic treatment. The beaker was then transferred to a magnetic
144 stirrer and constantly stirred for 4 h at 25 ºC. After that, the suspension was filtered
145 and filtration residue (Co^{2+} loaded SAM-SCS, Co-SAM-SCS) was washed with
146 ultrapure water for several times and dried in an oven at 80 ºC for 24 h. As a
147 comparison, Fe^{2+} loaded SAM-SCS (Fe-SAM-SCS) catalyst was also prepared
148 according to the above method, where Fe^{2+} was used to replace Co^{2+}.

149 *2.4. Characterization*

150 Characterization of the catalysts (SCS, SAM-SCS, Co-SAM-SCS) was
151 performed by using Brunauer–Emmett–Teller (BET), scanning electron microscopy
152 (SEM), energy dispersive X-ray spectroscopy (EDS), X-ray photoelectron spectrum
153 (XPS), X-ray diffraction (XRD), and Fourier transform infrared spectroscopy
154 (FT-IR).The specific surface area, pore volume and pore size of SCS, SAM-SCS and
155 Co-SAM-SCS were measured by the N_2-BET adsorption method (Micromeritics
156 Instrument Corporation, TRI-STAR3020, USA). The morphology of the catalysts was
157 examined by SEM scanning (Carl Zeiss, EVO-MA10, Germany). EDS of the samples
158 was performed with an energy dispersive X-ray detector (Oxford Instruments, UK).
159 The crystal structure of the catalysts was examined with a D/max-2500 X-ray
160 diffractometer (Rigaku, Japan) with Cu Kα radiation, testing in the region of 2θ from
161 5º to 80º. FTIR absorption spectra were obtained from a GX spectrophotometer
162 (Perkin Elmer, USA) with the standard KBr disk method. In addition, XPS was
163 adopted to investigate the chemical states of elements by using an Axis Ultra

spectrometer (Kratos, Japan) with Al Kα source ($h\nu$ = 1486.6 eV). In the electron paramagnetic resonance (EPR) measurements, 50 mL of solution was sampled out from the heterogeneous Fenton-like system and mixed with 5,5-Dimethyl-1-pyrroline-N-oxide (DMPO, 50 mM) to create DMPO–•OH adducts.

2.5. Adsorption Experiments

The adsorption characteristics of the prepared catalysts were evaluated by adsorption experiments using SMZ solution. The initial SMZ concentration used in this study was 5 mg/L. All batch experiments were performed in 250 mL flasks containing 100 mL of SMZ solution and 50 mg of SCS, SAM-SCS, Fe-SAM-SCS or Co-SAM-SCS, which were stirred in a water bath shaker at 160 rpm and 25 ± 0.5 °C. For certain time intervals, 0.5 mL of solution was sampled out for measurement of the concentration of SMZ. The adsorbed amount of SMZ was calculated as follow:

$$Q_t = (C_0 - C_t)\, V/m \quad (1)$$

Where Q_t is the adsorption quantity of SMZ on SCS, SAM-SCS or Co-SAM-SCS (mg/g); C_0 and C_t are the initial concentration and the measured concentration of SMZ (mg/L), respectively; m is the weight of SCS, SAM-SCS or Co-SAM-SCS (g) and V is the volume of SMZ solution (L).

The pseudo-first order kinetic model (2) (Lagergren 1898) and pseudo-second order kinetic model (3) (Ho and McKay 1998) were adopted to study the adsorption kinetics.

$$\log (Q_e - Q_t) = \log Q_e - k_f \cdot t /2.303 \quad (2)$$

$$t/Q_t = 1/k_s Q_e^2 + t/Q_e \quad (3)$$

Where Q_t and Qe are the adsorbed amount (mg/g) of SMZ on adsorbents at t and equilibrium, respectively. k_f is pseudo-first rate constant (1/h), and k_s is the pseudo-second rate constant (g/mg·h), respectively.

2.6. Fenton-like reaction

The heterogeneous Fenton-like reaction was performed in 250 mL glass conical flasks containing 100 mL of reaction solution at 25 °C and stirred at 160 rpm. SMZ concentration in all experiment groups was 50 mg/L. The initial pH of SMZ solution was set as 7.0 unless other mentioned. Typically, in the comparative degradation experiment, 50 mg of SCS, SAM-SCS, Fe-SAM-SCS or Co-SAM-SCS was added in 100 mL SMZ solution, and then a certain amount of H_2O_2 solution (30 wt%) was added to trigger the Fenton-like reactions. For certain time intervals, 0.5 mL of reaction solution was sampled out for measurement of the concentration of SMZ. In the preliminary experiment on the real wastewater treatment, tap water (derived from Changsha running-water company), river water (Xiangjiang River, Changsha, China) and municipal wastewater (obtained from Changsha 1st sewage treatment plant, Changsha, China) were used as the solution for the preparation of 50 mg/L SMZ wastewater. In these experiments, the catalyst loading is 0.7 g/L, H_2O_2 dosage is 4%, and the initial pH of the solution was adjusted to 9.0. The experiments were performed in 250 mL glass conical flasks containing 100 mL of reaction solution at 25 °C and stirred at 160 rpm. All the experiments (including the adsorption experiments) were performed in triplicate.

2.7. Analytical methods

208 The concentration of SMZ was measured according to a published method
209 (Teixido et al. 2013) by high performance liquid chromatography (HPLC, Agilent
210 1100 series, USA) with an Agilent TC-C18 column (4.6 × 250 mm, 5 μm). In addition,
211 SMZ mineralization was evaluated by detecting the TOC with a TOC-5000A model
212 analyzer (Shimadzu, Japan). The intermediates analysis was performed by an
213 ultra-high-performance liquid chromatography mass spectrometry (UPLC-MS,
214 Agilent 1290/6460, Triple Quad MS, USA) system equipped with an Symmetry C18
215 column (50 mm × 2.1 mm × 5 μm). The detailed description of detecting condition
216 was provided in supplementary material. Total iron concentration in the solution after
217 the reaction was determined using the 1, 10-phenanthroline-based method (HACH
218 method 8146) with a HACH DR2000 spectrophotometer (Hach, USA). Cobalt
219 concentration in the solution after the reaction was measured by flameless atomic
220 absorption spectroscopy (AAS, PEAA700, Perkin Elmer, USA). The filtrate of the
221 reaction solution was used in above mentioned measurements.

222 **3. Results and discussion**

223 *3.1. Physicochemical characterization of the prepared catalysts*

224 The prepared catalysts (SCS, SAM-SCS, Co-SAM-SCS and used-Co-SAM-SCS)
225 were characterized via different methods. Firstly, the surface properties of the
226 catalysts were investigated by BET analysis. We found that specific surface areas of
227 SCS increased from 67.14 to 179.62 m^2/g (Table S2) after SAM modification,
228 suggesting that SAM modification significantly changed the morphology of SCS. The

229 remarkable increase in specific surface area is because calcium silicate minerals in the
230 surface of SCS were selectively removed by SAM treatment, resulting in forming
231 irregular surfaces (Cheng et al. 2017a). Compared to SAM-SCS, Co-SAM-SCS
232 showed an even larger specific surface area, this could be ascribed to the fact that Co
233 formed new structure on the surface of SAM-SCS. Only a slight decrease was
234 observed in the surface areas of used-Co-SAM-SCS, indicated that no significant
235 change occurred in the morphology of SAM-SCS during the Fenton-like experiments.
236 On the other hand, the hysteresis of modified-SCS (SAM-SCS, Co-SAM-SCS and
237 used-Co-SAM-SCS) was observed (Fig. S1), indicating that the modified-SCS
238 presented the larger number of mesoporous compared to SCS.

239 SEM was applied to further study the morphologies changes of SCS. As seen
240 from Fig. 1a, the surface of SCS was relatively flat and smooth. After SAM
241 modification, there was an obvious change in the surface morphology of SCS. As
242 displayed in Fig. 1b, SAM-SCS presented irregular shapes and sizes. Fig. 1c revealed
243 that after Co^{2+} deposition SAM-SCS surface was covered by a rather uniform Co
244 layer. SEM image of used-Co-SAM-SCS is very similar to that of Co-SAM-SCS (Fig.
245 1c), further demonstrating that no significant change occurred in the morphology of
246 Co-SAM-SCS during the Fenton-like degradation experiments.

247 Additional elemental mappings combined with EDS analysis for the prepared
248 catalysts were also performed. EDS analysis showed that the unmodified SCS mainly
249 consists of O, Ca, Fe, Si, Mg, Mn and Al (Fig. S2a). After SAM modification, these
250 elements are still detected (Fig. S2b), but a distinct variation in the signals of them

was observed. As illustrated in Table S3, the content of Ca was remarkably decreased, while Fe content was increased after SAM modification. In particular, the mass ratio of Ca to Fe was decreased from 2.27 to 1.29 after SAM modification. The results from element mapping coincided well with the EDX analysis. For example, we can clearly see from Fig. 2 that the signal intensity of Ca gradually reduced after the modifications. The Co element distributed throughout the film of Co-SAM-SCS (Fig. 2O) and used-Co-SAM-SCS (Fig. 2T), suggesting that Co had been evenly dispersed on the surface of SAM-SCS and maintained good stability.

XRD diffraction patterns of SCS, SAM-SCS, Co-SAM-SCS and used-Co-SAM-SCS were obtained to evaluate the modification of SCS with SAM and Co^{2+} (Fig. 3). As can be seen in Fig. 3a, the intensities of dicalcium silicate peaks (2θ; 32.02º and 32.92º, JCPDS 77-0409) prominently decreased after SAM modification. On the contrary, the intensities of iron oxide peaks (2θ; 36.21º, 42.07º and 61.16º, JCPDS 74-1880) of SAM-SCS were enhanced as compared to those of unmodified SCS. XRD analysis indicated that the SAM modification removed a portion of calcium silicate minerals from SCS. As for SAM-SCS and Co-SAM-SCS, the similar XRD patterns were found (Fig. 3). That is to say, the introduction of Co in the catalyst had no noticeable influence on its crystalline structure. The peaks for CoO (2θ; 36.37º, 42.26º and 61.38º, JCPDS 48-1719) were found in Co-SAM-SCS, suggesting that Co was successfully introduced onto the surface of SAM-SCS. No obvious decline in Co peaks after 5 cycles of degradation test revealed that a negligible amount of Co on the surface of SAM-SCS was lost during the Fenton-like processes. The decrease in the

peak at 2θ values of 29.36º belongs to $CaCO_3$ (JCPDS 05-0586) in Co-SAM-SCS and used-Co-SAM-SCS may attribute to that part of $CaCO_3$ in SAM-SCS was removed under acidic condition during the preparation of Co-SAM-SCS.

The structure of the catalysts was also studied by FT-IR spectra. As displayed in Fig. 3b, the FT-IR spectra of SCS and SAM-modified SCS are similar. The broad bands in the range of 1400-1500 cm^{-1} and 800-1000 cm^{-1} are primarily associated to the stretching vibrations of Ca−O (Gadsden 1975) and Si−O (Criado et al. 2007), respectively. The bands of Ca−O and Si−O decreased obviously after SAM modification, which was in agreement with XRD analysis. For Co-SAM-SCS, no discernable discrepancy was observed, which is likely due to the small amount of Co in the catalyst, and it also inferred that the introduction of Co has no impacts on the initial chemical structure of SAM-SCS.

Fig. 4A displays the comparison of the survey spectra of SCS and SAM-modified SCS. The elements of Si (102.3 eV), Ca (347.5 eV, 351.2 eV), Fe (711.7eV, 724.9 eV), O (531.1 eV) and Mg (1303.7 eV) can be clearly observed on the spectra of all the four samples, while the elements of Co can only be observed on the spectra of Co-SAM-SCS and used-Co-SAM-SCS. Fig. 4B and 4C present the high resolution XPS spectra of Ca and Fe, respectively. It can be clearly seen from Fig. 4B that Ca 2p peaks with the binding energy of 347.5 eV and 351.2 eV in SAM-SCS are much weaker than that in SCS, and these peaks in the spectra of Co-SAM-SCS and used-Co-SAM-SCS further decreased as compared to those in SAM-SCS. Fig. 4C shows the Fe 2p spectrum with two individual peaks located at 724.6 eV for Fe $2p_{1/2}$

295 and the other one with the binding energy of 711.7 eV is assigned to Fe $2p_{3/2}$. It was
296 found that Fe 2p peaks in the spectra of modified SCS (SAM-SCS, Co-SAM-SCS and
297 used-Co-SAM-SCS) were enhanced as compared with those in the spectra of SCS.
298 We found there was no discernable change in the XPS spectra of Co for
299 Co-SAM-SCS and used-Co-SAM-SCS (Fig. 4D). Two major peaks with binding
300 energies at 797.6 eV and 781.6 eV are attributed to Co $2p_{3/2}$ and Co $2p_{1/2}$ of Co, and
301 the satellite peaks were found at 786.4 eV and 803.7 eV (Li et al. 2016). Overall the
302 XPS results coincided well with the SEM, EDS, and XRD analysis.

303 *3.2. Adsorption of SMZ by the catalysts*

304 The adsorption of organic pollutants onto the surface of catalysts are important
305 for the catalytic degradation since the heterogeneous Fenton-like degradation mainly
306 occurs at the solid–liquid interface (Xie et al. 2014). Thus, in the first step, the
307 adsorption of SMZ by SCS, SAM-SCS and Co-SAM-SCS was studied by using 5
308 mg/L of SMZ solution. As revealed in Fig. 5, the adsorption of SMZ increased
309 quickly in 30 min and achieved adsorption equilibrium within 2 h in all three studied
310 systems. Fig. 5 demonstrates that the adsorption performance of Co-SAM-SCS is
311 similar to that of SAM-SCS, whereas SCS shows much lower adsorption capability.
312 The remarkable adsorption rate can be ascribed to the changes of surface structure and
313 chemical composition of SCS. As shown in Table S2 and Fig. 1, the surface area, total
314 porosity and total pore volume of SCS increased largely after SAM modification.
315 Further study showed that the sorption kinetics of SMZ on SCS, SAM-SCS and
316 Co-SAM-SCS can be well fitted by pseudo-second order kinetic model (R^2 = 0.9995,

317 0.9994 and 0.9997, respectively), suggesting chemisorption is the rate-limiting step
318 for sorption (Brusseau et al. 1991, Gong et al. 2009, Xu et al. 2012).

319 *3.3. Comparative degradation behavior of SMZ in different Fenton-like systems*

320 Degradation behaviors of SMZ were investigated by homogeneous and
321 heterogeneous Fenton-like processes to evaluate the catalytic activity of
322 Co-SAM-SCS (Fig. 6). The degradation experiments were conducted at pH 7.0 with
323 50 mg/L of SMZ solution. Fig. 6a illustrated that the degradation rates of SMZ were
324 very different to each other in these systems. It was found that 4.79% of SMZ was
325 removed in the SCS/H_2O_2 system within the first 1 h and then the concentration of
326 SMZ did not significantly change during the subsequent 3 h (Fig. 6a). The SAM
327 modification enhanced the catalytic ability of SCS, approximately 20% degradation
328 efficiency enhancement, which mainly due to the reduction of calcium mineral and
329 the formation of higher surface area. What's more, the removal rate of SMZ could
330 reach to 77.62% when Co^{2+} was introduced to SAM-SCS.

331 For comparison, $Co(NO_3)_2$ and Fe-SAM-SCS were also taken into consideration.
332 As shown in Fig. 6a, the efficiency of heterogeneous Co^{2+}/H_2O_2 Fenton-like process
333 was relatively low, only 12.56% of SMZ was degraded in 240 min. This is because
334 high H_2O_2 concentration ($H_2O_2/Co^{2+} = 6$) is required to achieve efficient oxidation in
335 heterogeneous Co^{2+}/H_2O_2 system (Bokare and Choi 2014, Ling et al. 2010).
336 Compared with SAM-SCS, Fe-SAM-SCS exhibited higher catalytic activity and SMZ
337 concentration was reduced by 31.63%. However, this value is not comparable with
338 that of Co-SAM-SCS, which could be ascribed to the fact that Fe-based

Fenton/Fenton-like reactions are more efficient at acidic condition. Over all, the corresponding degradation rates of all the catalysts were in the following order: Co-SAM-SCS > Fe-SAM-SCS > SAM-SCS > $Co(NO_3)_2$ > SCS. Besides, these results are in good accordance with the results of TOC analysis (Fig. 6b), demonstrating that Co-SAM-SCS has high potential in practical applications.

3.4. Effects of catalyst loading, H_2O_2 dosage and pH on SMZ degradation

The effects of catalyst concentration on the degradation rates of SMZ were evaluated by performing experiments with the presence of increasing amounts of Co-SAM-SCS. As seen in Fig. 7a, SMZ removal in 240 min increased from 29.31% to 82.57% along with the increase of catalyst dosage from 0.1 to 0.7 g/L. This is probably due to that the number of active sites increased as the increased Co-SAM-SCS loadings, which accelerated the decomposition of H_2O_2 and the generation of HO•. On the other hand, the decline in SMZ removal was observed when increasing Co-SAM-SCS loading up to 1.0 g/L. The probable reason was that the excessive Co-SAM-SCS decreased the density of surface adsorbed H_2O_2, and reduced the concentration of HO• on the solid-liquid inter-surface (Wang et al. 2016). Besides, there also research suggested that iron surfaces would then cause the undesirable consumption of radicals (e.g., HO• and HOO•) through the following equations (Cheng et al. 2014, Hu et al. 2011b, Huang et al. 2012).

$$\equiv Fe(II) + HO\bullet \rightarrow \equiv Fe(III) + OH^- \quad (4)$$

$$\equiv Fe(III) + HO_2\bullet \rightarrow \equiv Fe(II) + HO_2^- \quad (5)$$

The effect of H_2O_2 dosage (0% to 6%) on the degradation of SMZ was then

examined. The experimental results (Fig. 7b) showed the removal of SMZ was quite limited (less than 5%) in the absence of H_2O_2. In fact, this part of SMZ was removed by the adsorption of Co-SAM-SCS. The introduction of H_2O_2 into the SMZ solution significantly accelerated the removal of SMZ. The degradation rate of SMZ increased along with the increase of H_2O_2 dosage from 1% to 4%, indicating that the concentration of H_2O_2 was directly related to the degradation of SMZ. That makes sense, because H_2O_2 is directly involved in the generation of the reactive radicals. However, the degradation rate of SMZ decreased when the H_2O_2 dosage further increased to 6%, which is possibly due to the scavenging of HO• by excessive H_2O_2 through equation (6) and (7) (Hu et al. 2011a, Huang et al. 2008, Xia et al. 2011).

$$H_2O_2 + HO\bullet \rightarrow HO_2\bullet + H_2O \quad (6)$$

$$HO_2\bullet + HO\bullet \rightarrow O_2 + H_2O \quad (7)$$

It has been well established that pH of the solution plays a critical role in the efficiency of the Fenton/Fenton-like oxidation. In the tested pH range (5-9), at least 60% of SMZ can be degraded after 240 min, suggesting that Co-SAM-SCS could be used for degradation of organic contaminants over a wide range of pH values. As illustrated in Fig. 7c, the degradation efficiency increased gradually as pH increased from 5.0 to 9.0, which indicated that the increase of pH favored the catalytic degradation of SMZ in the Co-SAM-SCS/H_2O_2 system. This result would be ascribed to the fact that Co rather than Fe played the major role in the catalytic degradation of SMZ under low pH condition. In this regard, the Co-SAM-SCS catalyzed heterogeneous Fenton-like process showed a remarkable advantage due to the

383 working environment.

384 *3.5. Identification of the dominant radicals*

385 It has been widely accepted that the degradation of pollutants is attributed to the
386 generation of radicals originated from the activation of H_2O_2 in the Fenton/
387 Fenton-like process (Centi and Perathoner 2003). In order to elucidate the reaction
388 mechanism in depth, the dominant radical that contributes to the degradation of SMZ
389 was identified by free radical trapping experiments. In this study, tert-butyl alcohol
390 (TBA) was utilized for hydroxyl radical (HO•) scavenger and 1,4-benzoquinone (BQ)
391 was used for superoxide radical ($\bullet O_2^-$) scavenger (Feng et al. 2010, Ozcan et al. 2017).
392 As seen from Fig. 8a, addition of BQ caused a slight decrease in the degradation rate
393 of SMZ, indicating that $O_2\bullet^-$ played a minor role in SMZ degradation. On the other
394 hand, TBA caused prominently deactivation of the Co-SAM-SCS catalyst. The
395 degradation rate of SMZ declined from 96.72% to 37.13% in the presence of 20 mM
396 of TBA, which demonstrated the crucial role of HO• in the catalytic degradation
397 process. According to these results, it can be concluded that the major active specie in
398 this heterogeneous Fenton-like reaction should be HO•. The formation of HO• was
399 also verified by EPR spin trapping experiment. Fig. 8b reveals that HO• were
400 generated in Co-SAM-SCS/H_2O_2 and SAM-SCS/H_2O_2 systems. The intensity of the
401 generated HO• was found to be almost 3 times higher for Co-SAM-SCS than for
402 SAM-SCS. These results were consistent with the observed enhancement in SMZ
403 removal.

3.6. Possible activation mechanisms of H_2O_2

It is generally accepted that in iron oxides based Fenton oxidation systems, HO• is believed to be generated by the decomposition of H_2O_2 on the surface of the heterogeneous catalyst through Eqs. (8) and (9) (Zhao et al. 2017). In these processes, Fe(II) is produced via reduction of Fe(III), while HO• is continuously generated from the decomposition of H_2O_2. Meanwhile, it should be noted that competitive reactions (e.g., Eqs. (1) and (2)) could occur (Hu et al. 2011b, Huang et al. 2012, Zhang et al. 2007), which negatively influence the Fenton process.

$$\equiv Fe(II) + H_2O_2 \rightarrow \equiv Fe(III) + HO\bullet \quad (8)$$

$$\equiv Fe(III) + H_2O_2 \rightarrow \equiv Fe(II) + H^+ + HO_2\bullet \quad (9)$$

By contrast, the generation of HO• by Co^{2+}-mediated activation of H_2O_2 has been documented only in a few studies. Based on previous researches (Bokare and Choi 2014, Shen et al. 2017) and the experimental results obtained in this work, a possible HO• formation mechanism by Co can be proposed as Eqs. (10-12). Very interesting, HO_2^- produced in the competitive reaction (Eq. (5)) of iron based Fenton processes, plays an important role in the reduction of Co(III) (Eq. 12). What's more, HO_2• generated from Eqs. (9) and (12) can react with Fe(III) to produce HO_2^- via Eq. (5). That is to say, Co and Fe on the surface of Co-SAM-SCS present synergistic effects on the efficient generation of HO• (Fig. 9).

$$\equiv Co(II) + H_2O_2 \rightarrow \equiv Co(III) + HO\bullet \quad (10)$$

$$H_2O_2 + HO^- \leftrightarrow HO_2^- + H_2O \quad (11)$$

$$\equiv Co(III) + HO_2^- \rightarrow \equiv Co(II) + HO_2\bullet \quad (12)$$

As shown in Eq. (11), HO^- plays an important role in the Co(II)/Co(III) circulation, which has been varied by our result in section 3.3 that the Co-SAM-SCS catalyst exhibited better catalytic performance in alkaline solutions (pH = 9) than acidic solution (pH = 5). At higher pH, a larger number of perhydroxyl anions (HO_2^-) were present in the solution (Eq. (11)). Compared with H_2O_2 molecules, HO_2^- is more nucleophilic and show higher activity to interact with Co(III) in the Co-SAM-SCS catalyst (Eq. (12)) (Nguyen et al. 2013).

3.7. Degradation intermediates and pathway of the SMZ degradation

To fully understand the degradation process of SMZ by the Co-SAM-SCS catalyzed Fenton-like reaction, LC-MS analyses were further performed to identify the oxidation products of SMZ. The LC patterns showed that intensity of SMZ peak (3.52 min) decreased quickly after H_2O_2 was added to the system (Fig. 10a). Meanwhile, two peaks emerged between 0.60 min and 1.10 min, and the intensity of them increased gradually with the reaction time. In our study, three main degradation intermediates of SMZ were detected by LC-MS, which included N-(4,6-dimethylpyrimidin-2yl)benzene-1,4-diamine (A, *m/z* 215), 4-aminophenol (B, *m/z* 110) and 4,6-dimethylpyrimidin-2-ol (C, *m/z* 125) (Fig. S3). Further, we found that A was the dominant product at 60 min, but C became the most abundant product after 120 min. On the basis of these information and the studies (Guo et al. 2013, Li et al. 2017) published previously, a possible degradation pathway of SMZ in the Co-SAM-SCS/H_2O_2 system was proposed in Fig. 10b. First, SO_2 elimination driven by HO• led to the formation of A, which is a phenomenon frequently observed in the

448 degradation of sulfonamides (Boreen et al. 2005, Huang et al. , Neafsey et al. 2010).
449 Then, C−N bond on the benzene ring was cleaved to form the degradation products of
450 B and C. Finally, B and C could be further attacked by HO•, leading to the formation
451 of harmless inorganic species and small-molecule organic acids.

452 *3.8. The stability and the degradation of SMZ in natural samples*

453 The stability of the catalyst is an important issue that should be considered
454 before actual application. The reusability is commonly used for evaluating the
455 stability of Co-SAM-SCS. As shown in Fig. 11, the degradation efficiency was nearly
456 maintained at the level of fresh sample after five successive runs. Furthermore, the
457 structural stability of the Co-SAM-SCS catalyst was examined by SEM (Fig. 1), EDS
458 (Fig. 2), XRD (Fig. 3) and XPS (Fig. 4), as can be seen, the crystal structure and
459 morphology of used-Co-SAM-SCS are very similar to those of fresh Co-SAM-SCS.
460 In addition, the leached Co and Fe after reaction were only 2.36 mg/L and 0.17 mg/L,
461 respectively.

462 In real applications, the composition of actual wastewater is extremely complex.
463 Therefore, huge differences could be obtained between removal efficiencies in a
464 simulated wastewater and an actual polluted wastewater. In this work, the removal
465 efficiency of SMZ by Co-SAM-SCS/H_2O_2 was studied using ultrapure water, tap
466 water (Changsha Running-water Company), river water (taken from Xiangjiang River,
467 Changsha), and municipal wastewater (obtained from Changsha 1st sewage treatment
468 plant, China). The results showed that, after the Fenton-like process, more than 95%
469 of SMZ is removed by Co-SAM-SCS/H_2O_2 for ultrapure water, ultrapure water and

river water (Fig. S4). While relatively lower removal of SMZ (about 86%) was observed in wastewater, this is probably due to the competition of HO• by the abundant organic matters in municipal wastewater. The obtained results greatly suggested that this novel catalyst exhibited good stability, and also has a great potential for practical treatment of real wastewater. The versatility of this Co-SAM-SCS/H_2O_2 system is also enhanced by the fact that it can work efficiently in neutral or slightly basic pH condition. More importantly, the catalyst can be recovered by a simple settling and separation process, which enables the reuse of the catalyst.

3.9. Operating cost-efficiency comparison

The raw materials and chemicals used in the preparation of Co-SAM-SCS can be cheaply provided by the industrial supplies. The wholesale price of grinded SCS, salicylic acid, methanol, $Co(NO_3)_2{\cdot}6H_2O$ and H_2O_2 (30%) is about 0.15 US$/kg, 1.5 US$/kg, 0.4 US$/L, 1.8 US$/kg and 0.22 US$/L, respectively. In this study, the cost for the production of Co-SAM-SCS is about 1.7 US$/kg. According to the preliminary results abstained in this work, the chemical cost for the treatment of 50 mg/L SMZ wastewater is about 19 US$/$m^3$, which is higher than the costs of some reported AOPs (Table 1) (Boczkaj and Fernandes 2017, Patil and Gogate 2015, Thanekar et al. 2018, Weng et al. 2013). For example, in a recent work, Thanekar et al. (2018) reported the total cost of a hydrodynamic cavitation/H_2O_2/O_3 system is 4.55 US$/$m^3$. The higher chemical cost in our study is mainly because relatively high H_2O_2 dosage (4%) was adopted for the fast degradation of SMZ at slightly basic pH condition. It should be noted that over 80% of SMZ can be removed in 240 min with 2% of H_2O_2 (Fig. 7).

Under this condition, the chemical cost can be reduced to 5.6 US$/$m^3$. Furthermore, the chemical cost can also be reduced by recycling the catalyst. As shown in Table 1, the studied process (Co-SAM-SCS/H_2O_2) is more economical than a recently reported sonication/ Fention-like process (Jaafarzadeh et al. 2018). If the studied Fenton-like process can be put into practical application, it will provide a feasible way to reuse SCS and also achieve excellent environmental benefit.

4. Conclusions

• In this study, a novel heterogeneous Fenton-like system with Co-SAM-SCS as the catalyst was developed for the degradation of antibiotic SMZ in wastewater.

• The Co-SAM-SCS/H_2O_2 system can work efficiently in neutral or slightly basic pH conditions. Furthermore, the catalyst showed good stability and reusability.

• Co and Fe on the surface of Co-SAM-SCS present synergistic effects on the efficient generation of HO•, which was mainly responsible for the degradation of SMZ.

• Three main degradation intermediates were detected during the degradation process, based on which a possible degradation pathway of SMZ in the Co-SAM-SCS/H_2O_2 system was proposed.

• A further study conducted in three kinds of wastewater confirmed the application feasibility of this heterogeneous Fenton-like process for wastewater treatment. Meanwhile, further research conducted with more complex wastewater is still needed before the full-scale implementation.

• Our findings provide useful information to develop efficient and cost-effective approaches to degrade organic pollutants in wastewater.

Acknowledgements

This study was financially supported by the Program for the National Natural Science Foundation of China (51521006, 51579098, 51378190, 51408206), the National Program for Support of Top-Notch Young Professionals of China (2014), the Fundamental Research Funds for the Central Universities, Hunan Provincial Science and Technology Plan Project (No.2016RS3026), the Program for New Century Excellent Talents in University (NCET-13-0186), Shanghai Tongji Gao Tingyao Environmental Science and Technology Development Foundation, and the Program for Changjiang Scholars and Innovative Research Team in University (IRT-13R17).

References

Babić, S., Zrnčić, M., Ljubas, D., Ćurković, L., Škorić, I., 2015. Photolytic and thin TiO_2 film assisted photocatalytic degradation of sulfamethazine in aqueous solution. Environ. Sci. Pollut. Res. 22, 11372-11386.

Bai, Z., Yang, Q., Wang, J., 2016. Catalytic ozonation of sulfamethazine antibiotics using $Ce_{0.1}Fe_{0.9}OOH$: Catalyst preparation and performance. Chemosphere 161, 174-180.

Boczkaj, G., Fernandes, A., 2017. Wastewater treatment by means of advanced oxidation processes at basic pH conditions: A review. Chem. Eng. J. 320, 608-633.

Bokare, A.D., Choi, W., 2014. Review of iron-free Fenton-like systems for activating H_2O_2 in advanced oxidation processes. J. Hazard. Mater. 275, 121-135.

535 Boreen, A.L., Arnold, W.A., McNeill, K., 2005. Triplet-Sensitized Photodegradation
536 of Sulfa Drugs Containing Six-Membered Heterocyclic Groups: Identification of
537 an SO_2 Extrusion Photoproduct. Environ. Sci. Technol. 39 (10), 3630-3638.
538 Brusseau, M.L., Jessup, R.E., Rao, P.S.C., 1991. Nonequilibrium sorption of organic
539 chemicals: Elucidation of rate-limiting processes.
540 Burbano, A.A., Dionysiou, D.D., Suidan, M.T., Richardson, T.L., 2005. Oxidation
541 kinetics and effect of pH on the degradation of MTBE with Fenton reagent.
542 Water Res. 39 (1), 107-118.
543 Centi, G., Perathoner, S., 2003. Remediation of water contamination using catalytic
544 technologies. Appl. Catal., B: Environ. 41 (1–2), 15-29.
545 Cheng, M., Zeng, G., Huang, D., Lai, C., Liu, Y., Xu, P., Zhang, C., Wan, J., Hu, L.,
546 Xiong, W., Zhou, C., 2017a. Salicylic acid–methanol modified steel converter
547 slag as heterogeneous Fenton-like catalyst for enhanced degradation of alachlor.
548 Chem. Eng. J. 327, 686-693.
549 Cheng, M., Zeng, G., Huang, D., Lai, C., Liu, Y., Zhang, C., Wang, R., Qin, L., Xue,
550 W. and Song, B., 2018a. High adsorption of methylene blue by salicylic
551 acid-ethanol modified steel converter slag and evaluation of its mechanism. J.
552 Colloid Interf. Sci. 515,232-239
553 Cheng, M., Zeng, G., Huang, D., Lai, C., Xu, P., Zhang, C., Liu, Y., 2016a. Hydroxyl
554 radicals based advanced oxidation processes (AOPs) for remediation of soils
555 contaminated with organic compounds: A review. Chem. Eng. J. 284, 582-598.
556 Cheng, M., Zeng, G., Huang, D., Lai, C., Xu, P., Zhang, C., Liu, Y., Wan, J., Gong, X.,

Zhu, Y., 2016b. Degradation of atrazine by a novel Fenton-like process and assessment the influence on the treated soil. J. Hazard. Mater. 312, 184-191.

Cheng, M., Zeng, G., Huang, D., Liu, L., Zhao, M., Lai, C., Huang, C., Wei, Z., Li, N., Xu, P., Zhang, C., Li, F., Leng, Y., 2014. Effect of Pb^{2+} on the production of hydroxyl radical during solid-state fermentation of straw with *Phanerochaete chrysosporium*. Biochem. Eng. J. 84, 9-15.

Cheng, M., Zeng, G., Huang, D., Yang, C., Lai, C., Zhang, C., Liu, Y., 2018b. Tween 80 surfactant-enhanced bioremediation: toward a solution to the soil contamination by hydrophobic organic compounds. Crit. Rev. Biotechnol. 38(1), 17-30.

Cheng, M., Zeng, G., Huang, D., Yang, C., Lai, C., Zhang, C., Liu, Y., 2017b. Advantages and challenges of Tween 80 surfactant-enhanced technologies for the remediation of soils contaminated with hydrophobic organic compounds. Chem. Eng. J. 314, 98-113.

Cheng, Y., He, H., Yang, C., Zeng, G., Li, X., Chen, H., Yu, G., 2016c. Challenges and solutions for biofiltration of hydrophobic volatile organic compounds. Biotechnol. Adv. 34 (6), 1091-1102.

Criado, M., Fernández-Jiménez, A., Palomo, A., 2007. Alkali activation of fly ash: Effect of the SiO_2/Na_2O ratio. Micropor. Mesopor. Mater. 106 (1), 180-191.

Fan, H.-J., Huang, S.-T., Chung, W.-H., Jan, J.-L., Lin, W.-Y., Chen, C.-C., 2009. Degradation pathways of crystal violet by Fenton and Fenton-like systems: condition optimization and intermediate separation and identification. J. Hazard.

579 Mater. 171 (1), 1032-1044.
580 Fan, T., Liu, Y., Feng, B., Zeng, G., Yang, C., Zhou, M., Zhou, H., Tan, Z., Wang, X.,
581 2008. Biosorption of cadmium (II), zinc (II) and lead (II) by Penicillium
582 simplicissimum: Isotherms, kinetics and thermodynamics. J. Hazard. Mater. 160
583 (2), 655-661.
584 Feng, Y., Gong, J.-L., Zeng, G.-M., Niu, Q.-Y., Zhang, H.-Y., Niu, C.-G., Deng, J.-H.,
585 Yan, M., 2010. Adsorption of Cd (II) and Zn (II) from aqueous solutions using
586 magnetic hydroxyapatite nanoparticles as adsorbents. Chem. Eng. J. 162 (2),
587 487-494.
588 Gadsden, J.A., 1975 Infrared spectra of minerals and related inorganic c ompounds,
589 Butterworths.
590 Garoma, T., Umamaheshwar, S.K., Mumper, A., 2010. Removal of sulfadiazine,
591 sulfamethizole, sulfamethoxazole, and sulfathiazole from aqueous solution by
592 ozonation. Chemosphere 79(8), 814-820.
593 Gong, J.-L., Wang, B., Zeng, G.-M., Yang, C.-P., Niu, C.-G., Niu, Q.-Y., Zhou, W.-J.,
594 Liang, Y., 2009. Removal of cationic dyes from aqueous solution using magnetic
595 multi-wall carbon nanotube nanocomposite as adsorbent. J. Hazard. Mater. 164
596 (2), 1517-1522.
597 Guo, C., Xu, J., Wang, S., Zhang, Y., He, Y., Li, X., 2013. Photodegradation of
598 sulfamethazine in an aqueous solution by a bismuth molybdate photocatalyst.
599 Catal. Sci. Technol. 3 (6), 1603-1611.
600 Guo, J., Li, J., Chen, H., Bond, P.L., Yuan, Z., 2017. Metagenomic analysis reveals

601 wastewater treatment plants as hotspots of antibiotic resistance genes and mobile
602 genetic elements. Water Res. 123, 468-478.
603 Guo, S., Zhang, G.Wang, J., 2014. Photo-Fenton degradation of rhodamine B using
604 Fe_2O_3–Kaolin as heterogeneous catalyst: Characterization, process optimization
605 and mechanism. J. Colloid Interface Sci. 433, 1-8.
606 Ho, Y.S., McKay, G., 1998. Kinetic Models for the Sorption of Dye from Aqueous
607 Solution by Wood. Process Saf. Environ. Prot. 76 (2), 183-191.
608 Hu, X.-j., Wang, J.-s., Liu, Y.-g., Li, X., Zeng, G.-m., Bao, Z.-l., Zeng, X.-x., Chen,
609 A.-w.Long, F., 2011a. Adsorption of chromium (VI) by
610 ethylenediamine-modified cross-linked magnetic chitosan resin: isotherms,
611 kinetics and thermodynamics. J. Hazard. Mater. 185 (1), 306-314.
612 Hu, X., Liu, B., Deng, Y., Chen, H., Luo, S., Sun, C., Yang, P., Yang, S., 2011b.
613 Adsorption and heterogeneous Fenton degradation of 17α-methyltestosterone on
614 nano Fe_3O_4/MWCNTs in aqueous solution. Appl. Catal., B: Environ. 107 (3),
615 274-283.
616 Huang, D.-L., Zeng, G.-M., Feng, C.-L., Hu, S., Jiang, X.-Y., Tang, L., Su, F.-F.,
617 Zhang, Y., Zeng, W., Liu, H.-L., 2008. Degradation of lead-contaminated
618 lignocellulosic waste by Phanerochaete chrysosporium and the reduction of lead
619 toxicity. Environ. Sci. Technol. 42 (13), 4946-4951.
620 Huang, D., Hu, C., Zeng, G., Cheng, M., Xu, P., Gong, X., Wang, R., Xue, W., 2017.
621 Combination of Fenton processes and biotreatment for wastewater treatment and
622 soil remediation. Sci. Total Environ. 574, 1599-1610.

623 Huang, D., Liu, L., Zeng, G., Xu, P., Huang, C., Deng, L., Wang, R., Wan, J., The
624 effects of rice straw biochar on indigenous microbial community and enzymes
625 activity in heavy metal-contaminated sediment. Chemosphere 174, 545-553.
626 Huang, D., Xue, W., Zeng, G., Wan, J., Chen, G., Huang, C., Zhang, C., Cheng, M.,
627 Xu, P., 2016. Immobilization of Cd in river sediments by sodium alginate
628 modified nanoscale zero-valent iron: Impact on enzyme activities and microbial
629 community diversity. Water Res. 106, 15-25.
630 Huang, R., Fang, Z., Yan, X., Cheng, W., 2012. Heterogeneous sono-Fenton catalytic
631 degradation of bisphenol A by Fe3O4 magnetic nanoparticles under neutral
632 condition. Chem. Eng. J. 197, 242-249.
633 Jaafarzadeh, N., Takdastan, A., Jorfi, S., Ghanbari, F., Ahmadi, M., Barzegar, G., 2018.
634 The performance study on ultrasonic/Fe_3O_4/H_2O_2 for degradation of azo dye and
635 real textile wastewater treatment. J. Mol. Liq. 256, 462-470.
636 Kim, K.-S., Yang, C.-S., Mok, Y.S., 2013. Degradation of veterinary antibiotics by
637 dielectric barrier discharge plasma. Chem. Eng. J. 219, 19-27.
638 Lagergren, S., 1898. Zur theorie der sogenannten adsorption geloster stoffe. Kungliga
639 Svenska Vetenskapsakademiens. Handlingar 24, 1-39.
640 Lai, C., Wang, M.-M., Zeng, G.-M., Liu, Y.-G., Huang, D.-L., Zhang, C., Wang, R.-Z.,
641 Xu, P., Cheng, M., Huang, C., Wu, H.-P., Qin, L., 2016. Synthesis of surface
642 molecular imprinted TiO2/graphene photocatalyst and its highly efficient
643 photocatalytic degradation of target pollutant under visible light irradiation.
644 ApSS 390, 368-376.

Li, H., Wan, J., Ma, Y., Wang, Y., Chen, X., Guan, Z., 2016. Degradation of refractory dibutyl phthalate by peroxymonosulfate activated with novel catalysts cobalt metal-organic frameworks: Mechanism, performance, and stability. J. Hazard. Mater. 318, 154-163.

Li, M., Wang, C., Yau, M., Bolton, J.R., Qiang, Z., 2017. Sulfamethazine degradation in water by the VUV/UV process: Kinetics, mechanism and antibacterial activity determination based on a mini-fluidic VUV/UV photoreaction system. Water Res. 108, 348-355.

Ling, S.K., Wang, S., Peng, Y., 2010. Oxidative degradation of dyes in water using Co^{2+}/H_2O_2 and Co^{2+}/peroxymonosulfate. J. Hazard. Mater. 178 (1-3), 385-389.

Liu, Y., He, X., Fu, Y., Dionysiou, D.D., 2016. Degradation kinetics and mechanism of oxytetracycline by hydroxyl radical-based advanced oxidation processes. Chem. Eng. J. 284, 1317-1327.

Liu, Y., Hu, J. and Wang, J., 2014. Fe^{2+} enhancing sulfamethazine degradation in aqueous solution by gamma irradiation. Radiat. Phys. Chem. 96, 81-87.

Liu, Y. and Wang, J., 2013. Degradation of sulfamethazine by gamma irradiation in the presence of hydrogen peroxide. J. Hazard. Mater. 250-251, 99-105.

Liu, Y., Zeng, G., Zhong, H., Wang, Z., Liu, Z., Cheng, M., Liu, G., Yang, X., Liu, S., 2017. Effect of rhamnolipid solubilization on hexadecane bioavailability: enhancement or reduction? J. Hazard. Mater. 322, 394-401.

Mahamallik, P., Pal, A., 2016. Photo-Fenton process in a Co(II)-adsorbed micellar soft-template on an alumina support for rapid methylene blue degradation. Rsc

667 Advances 6 (103), 100876-100890.
668 Mahamallik, P., Pal, A., 2017. Degradation of textile wastewater by modified
669 photo-Fenton process: Application of Co(II) adsorbed surfactant-modified
670 alumina as heterogeneous catalyst. J. Environ. Chem. Eng. 5 (3), 2886-2893.
671 Navalon, S., Alvaro, M., Garcia, H., 2010. Heterogeneous Fenton catalysts based on
672 clays, silicas and zeolites. Appl. Catal., B: Environ. 99 (1), 1-26.
673 Neafsey, K., Zeng, X., Lemley, A.T., 2010. Degradation of Sulfonamides in Aqueous
674 Solution by Membrane Anodic Fenton Treatment. J. Agric. Food Chem. 58 (2),
675 1068-1076.
676 Nguyen, T.T.M., Park, H.-J., Kim, J.Y., Kim, H.-E., Lee, H., Yoon, J., Lee, C., 2013.
677 Microbial Inactivation by Cupric Ion in Combination with H_2O_2: Role of
678 Reactive Oxidants. Environ. Sci. Technol. 47 (23), 13661-13667.
679 Ozcan, A., Ozcan, A.A., Demirci, Y., Sener, E., 2017. Preparation of Fe_2O_3 modified
680 kaolin and application in heterogeneous electro-catalytic oxidation of enoxaciri.
681 Appl. Catal., B: Environ. 200, 361-371.
682 Patil, P.N. and Gogate, P.R., 2015. Degradation of dichlorvos using hybrid advanced
683 oxidation processes based on ultrasound. J. Water Process Eng. 8, 58-65.
684 Shen, Y., Zhou, Y., Zhang, Z., Xiao, K., 2017. Cobalt–copper oxalate nanofibers
685 mediated Fenton degradation of Congo red in aqueous solutions. J. Ind. Eng.
686 Chem. 52, 153-161.
687 Sopaj, F., Oturan, N., Pinson, J., Podvorica, F., Oturan, M.A., 2016. Effect of the
688 anode materials on the efficiency of the electro-Fenton process for the

689 mineralization of the antibiotic sulfamethazine. Appl. Catal., B: Environ. 199,
690 331-341.
691 Tang, L., Zeng, G.-M., Shen, G.-L., Li, Y.-P., Zhang, Y., Huang, D.-L., 2008. Rapid
692 detection of picloram in agricultural field samples using a disposable
693 immunomembrane-based electrochemical sensor. Environ. Sci. Technol. 42 (4),
694 1207-1212.
695 Teixido, M., Hurtado, C., Pignatello, J.J., Beltran, J.L., Granados, M., Peccia, J., 2013.
696 Predicting Contaminant Adsorption in Black Carbon (Biochar) Amended Soil for
697 the Veterinary Antimicrobial Sulfamethazine. Environ. Sci. Technol. 47 (12),
698 6197-6205.
699 Thanekar, P., Panda, M., Gogate, P.R., 2018. Degradation of carbamazepine using
700 hydrodynamic cavitation combined with advanced oxidation processes. Ultrason.
701 Sonochem. 40 (Part A), 567-576.
702 Wan, Z., Hu, J., Wang, J., 2016. Removal of sulfamethazine antibiotics using
703 CeFe-graphene nanocomposite as catalyst by Fenton-like process. J.Environ.
704 Manage.182, 284-291.
705 Wan, Z., Wang, J., 2017. Degradation of sulfamethazine using Fe_3O_4-Mn_3O_4/reduced
706 graphene oxide hybrid as Fenton-like catalyst. J. Hazard. Mater. 324 (Part B),
707 653-664.
708 Wang, M., Fang, G., Liu, P., Zhou, D., Ma, C., Zhang, D., Zhan, J., 2016.
709 Fe_3O_4@β-CD nanocomposite as heterogeneous Fenton-like catalyst for enhanced
710 degradation of 4-chlorophenol (4-CP). Appl. Catal., B: Environ. 188, 113-122.

711 Wang, Y., Feng, C., Li, Y., Gao, J., Yu, C.-P., 2017. Enhancement of emerging
712 contaminants removal using Fenton reaction driven by H_2O_2-producing
713 microbial fuel cells. Chem. Eng. J. 307, 679-686.
714 Weng, C.-H., Lin, Y.-T., Yuan, H.-M., 2013. Rapid decoloration of Reactive Black 5
715 by an advanced Fenton process in conjunction with ultrasound. Sep. Purif.
716 Technol. 117, 75-82.
717 Xia, M., Long, M., Yang, Y., Chen, C., Cai, W., Zhou, B., 2011. A highly active
718 bimetallic oxides catalyst supported on Al-containing MCM-41 for Fenton
719 oxidation of phenol solution. Appl. Catal., B: Environ. 110, 118-125.
720 Xie, Y., Yan, B., Xu, H., Chen, J., Liu, Q., Deng, Y., Zeng, H., 2014. Highly
721 Regenerable Mussel-Inspired Fe_3O_4@Polydopamine-Ag Core-Shell
722 Microspheres as Catalyst and Adsorbent for Methylene Blue Removal. Acs Appl.
723 Mater. Int. 6 (11), 8845-8852.
724 Xu, P., Zeng, G.M., Huang, D.L., Feng, C.L., Hu, S., Zhao, M.H., Lai, C., Wei, Z.,
725 Huang, C., Xie, G.X., 2012. Use of iron oxide nanomaterials in wastewater
726 treatment: a review. Sci. Total Environ. 424, 1-10.
727 Yang, C., Chen, H., Zeng, G., Yu, G., Luo, S., 2010. Biomass accumulation and
728 control strategies in gas biofiltration. Biotechnol. Adv. 28 (4), 531-540.
729 Yang, Y., Lu, X., Jiang, J., Ma, J., Liu, G., Cao, Y., Liu, W., Li, J., Pang, S., Kong, X.,
730 Luo, C., 2017. Degradation of sulfamethoxazole by UV, UV/H_2O_2 and
731 UV/persulfate (PDS): Formation of oxidation products and effect of bicarbonate.
732 Water Res. 118, 196-207.

733 Yang, Y., Pignatello, J.J., Ma, J., Mitch, W.A., 2016. Effect of matrix components on
734 UV/H_2O_2 and UV/$S_2O_8^{2-}$ advanced oxidation processes for trace organic
735 degradation in reverse osmosis brines from municipal wastewater reuse facilities.
736 Water Res. 89, 192-200.
737 Yap, P.-S., Cheah, Y.-L., Srinivasan, M., Lim, T.-T., 2012. Bimodal N-doped
738 P25-TiO_2/AC composite: Preparation, characterization, physical stability, and
739 synergistic adsorptive-solar photocatalytic removal of sulfamethazine. Appl.
740 Catal. A: Gen. 427–428, 125-136.
741 Yi, H., Xu, G., Cheng, H., Wang, J., Wan, Y., Chen, H., 2012. An overview of
742 utilization of steel slag. Procedia Environ. Sci. 16, 791-801.
743 Zeng, G., Chen, M., Zeng, Z., 2013a. Risks of neonicotinoid pesticides. Sci. 340
744 (6139), 1403-1403.
745 Zeng, G., Chen, M., Zeng, Z., 2013b. Shale gas: surface water also at risk. Nature 499
746 (7457), 154-154.
747 Zhang, C., Lai, C., Zeng, G., Huang, D., Yang, C., Wang, Y., Zhou, Y., Cheng, M.,
748 2016. Efficacy of carbonaceous nanocomposites for sorbing ionizable antibiotic
749 sulfamethazine from aqueous solution. Water Res. 95, 103-112.
750 Zhang, Y., Zeng, G.-M., Tang, L., Huang, D.-L., Jiang, X.-Y., Chen, Y.-N., 2007. A
751 hydroquinone biosensor using modified core-shell magnetic nanoparticles
752 supported on carbon paste electrode. Biosens. Bioelectron. 22 (9-10), 2121-2126.
753 Zhao, H., Chen, Y., Peng, Q., Wang, Q., Zhao, G., 2017. Catalytic activity of
754 MOF(2Fe/Co)/carbon aerogel for improving H_2O_2 and OH generation in solar

photo–electro–Fenton process. Appl. Catal., B: Environ. 203, 127-137.

Zhou, T., Wu, X., Mao, J., Zhang, Y., Lim, T.-T. , 2014. Rapid degradation of sulfonamides in a novel heterogeneous sonophotochemical magnetite-catalyzed Fenton-like (US/UV/Fe_3O_4/oxalate) system. Appl. Catal., B: Environ. 160-161, 325-334.

Zhou, T., Wu, X., Zhang, Y., Li, J., Lim, T.-T., 2013. Synergistic catalytic degradation of antibiotic sulfamethazine in a heterogeneous sonophotolytic goethite/oxalate Fenton-like system. Appl. Catal., B: Environ. 136, 294-30[illegible].

764

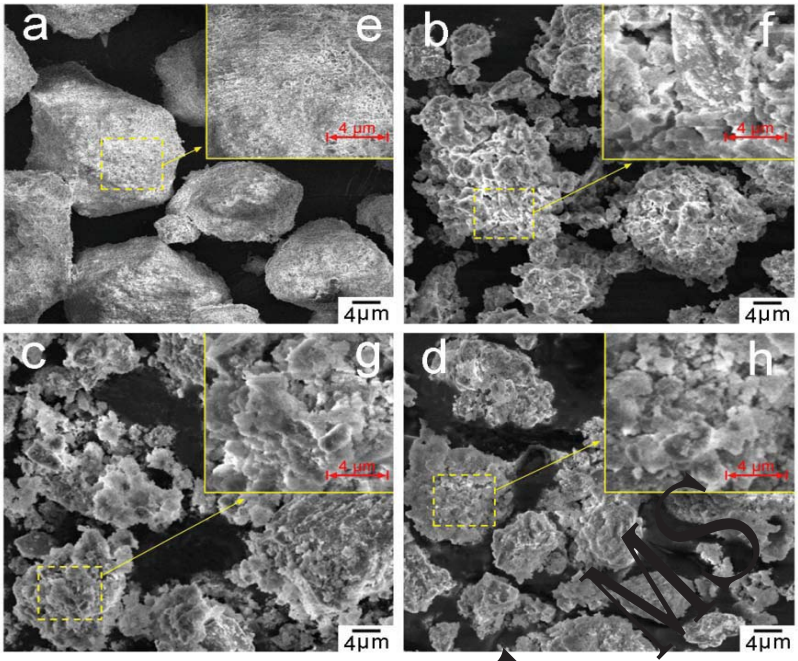

765

766 Fig. 1. SEM images of SCS (a), SAM-SCS (b), Co-SAM-SCS (c) and

767 Used-Co-SAM-SCS (d), and the enlarged SEM images of SCS (e), SAM-SCS (f),

768 Co-SAM-SCS (g) and Used-Co-SAM-SCS (h).

769

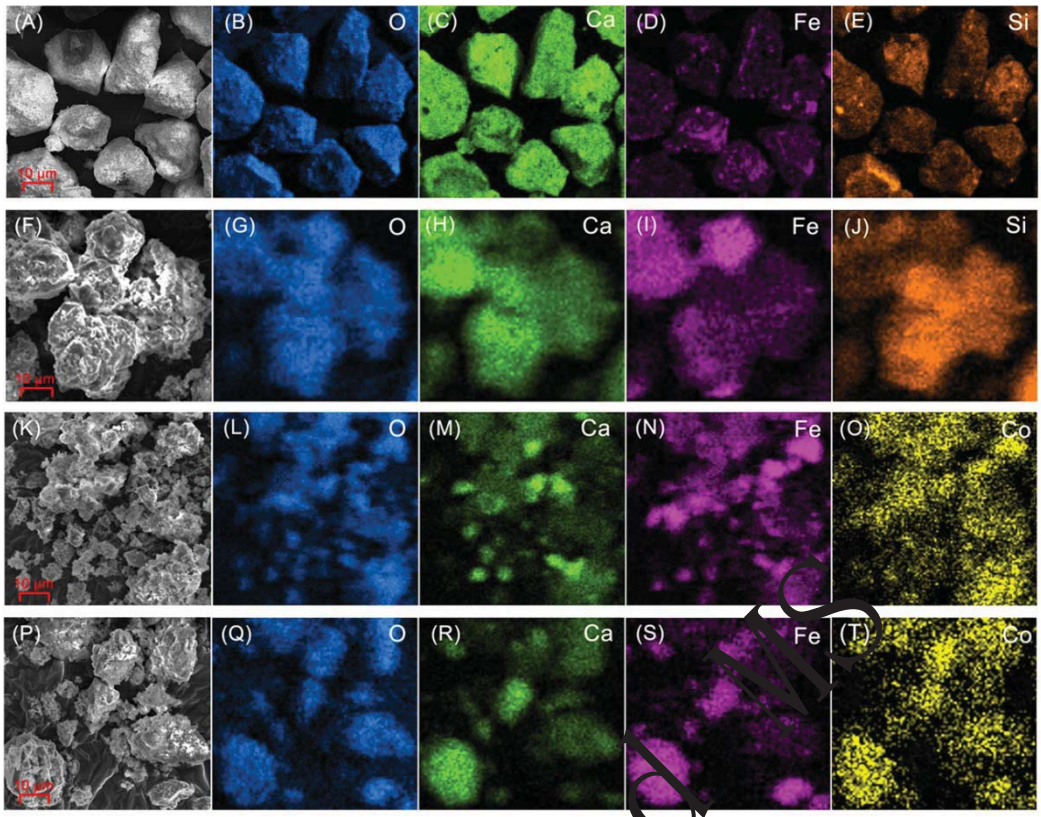

770

771 Fig. 2. SEM-EDS elemental mapping images of SCS (A-E), SAM-SCS (F-J),

772 Co-SAM-SCS (K-O) and Used-Co-SAM-SCS (P-T).

773

774

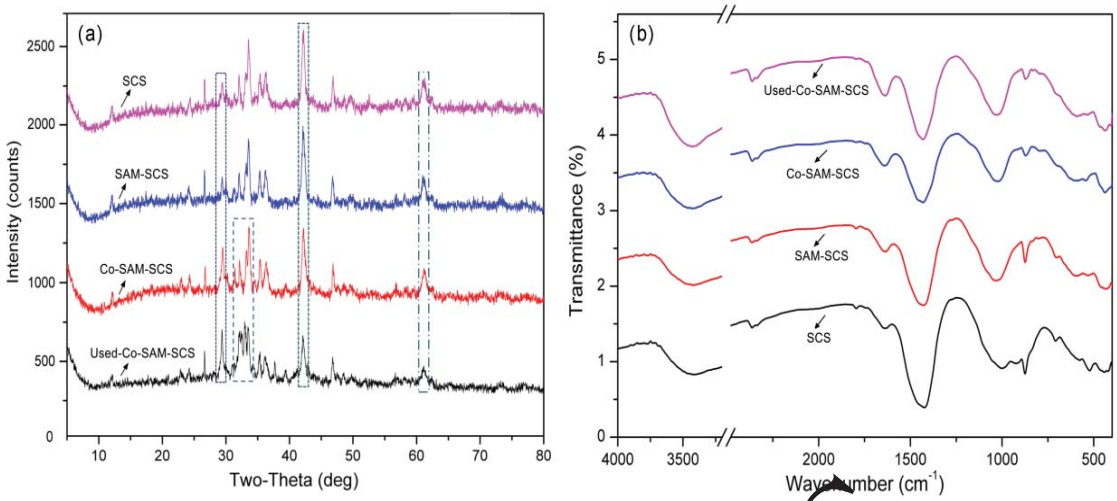

775

776 Fig. 3. XRD patterns (a) and FTIR absorption spectra (b) of SCS, SAM-SCS,

777 Co-SAM-SCS and Used-Co-SAM-SCS.

778

779

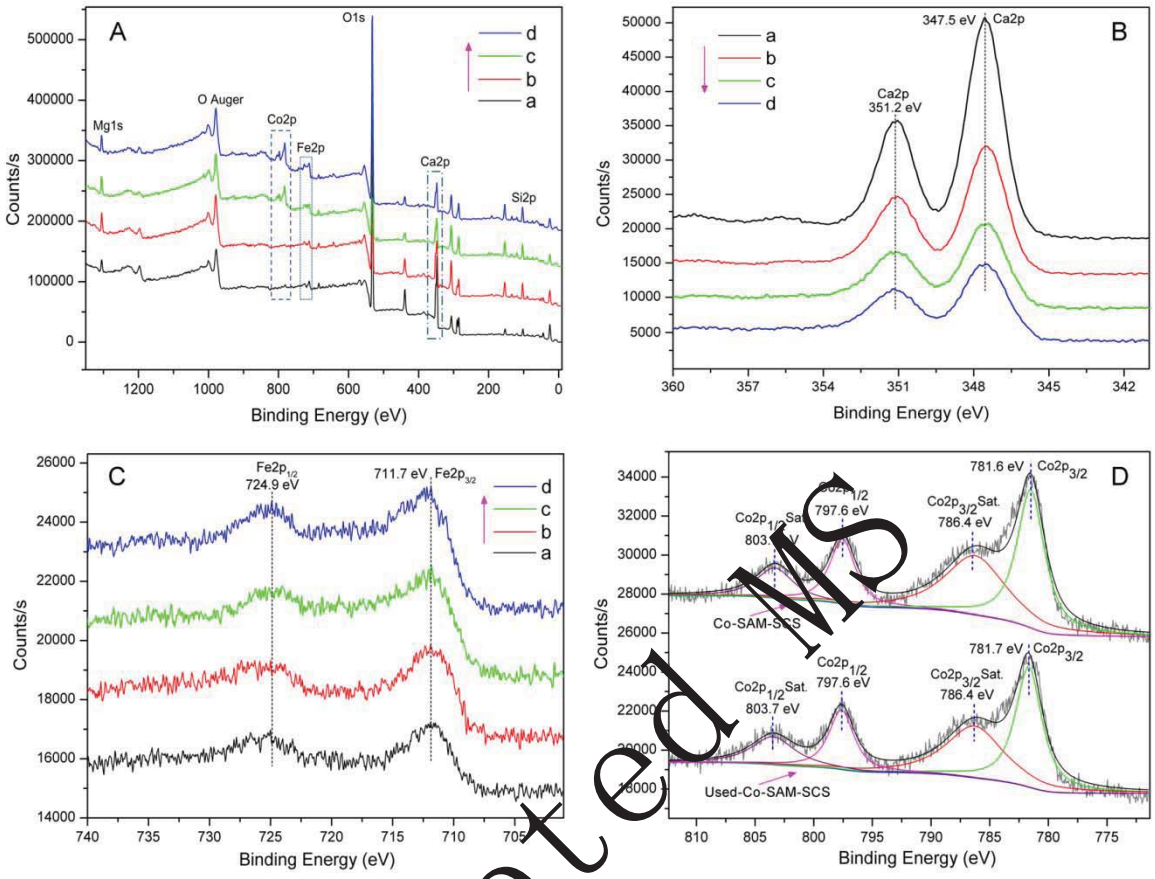

780

781 Fig. 4. XPS spectra of the SCS-based catalysts: (A) survey, (B) Ca 2p, (C) Fe 2p and

782 (D) Co 2p. (a): SCS, (b): SAM-SCS, (c): Co-SAM-SCS, (d) used-Co-SAM-SCS.

783

784

785

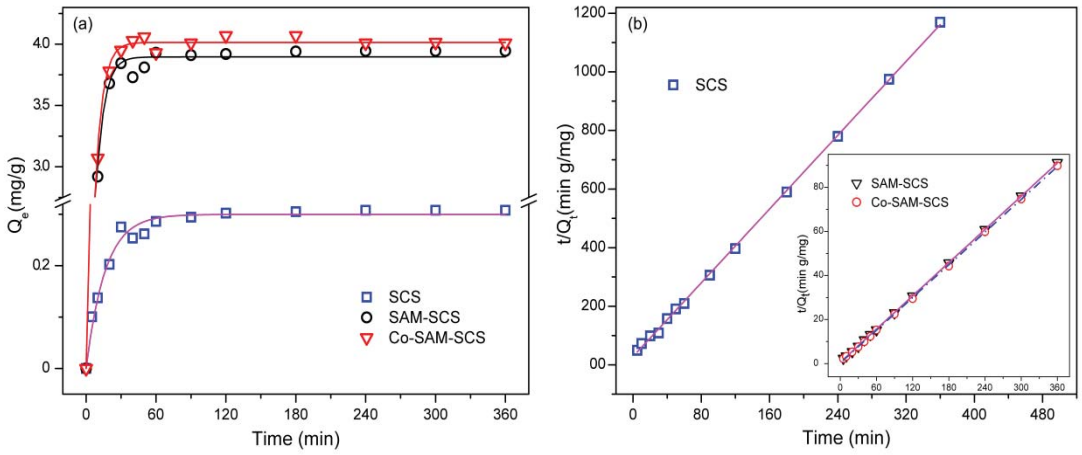

786

787 Fig. 5. The sorption kinetics of SMZ on SCS SAM-SCS and Co-SAM-SCS. (a) fitted

788 by pseudo-first order kinetic; (b) fitted by pseudo-second order kinetic.

789

790

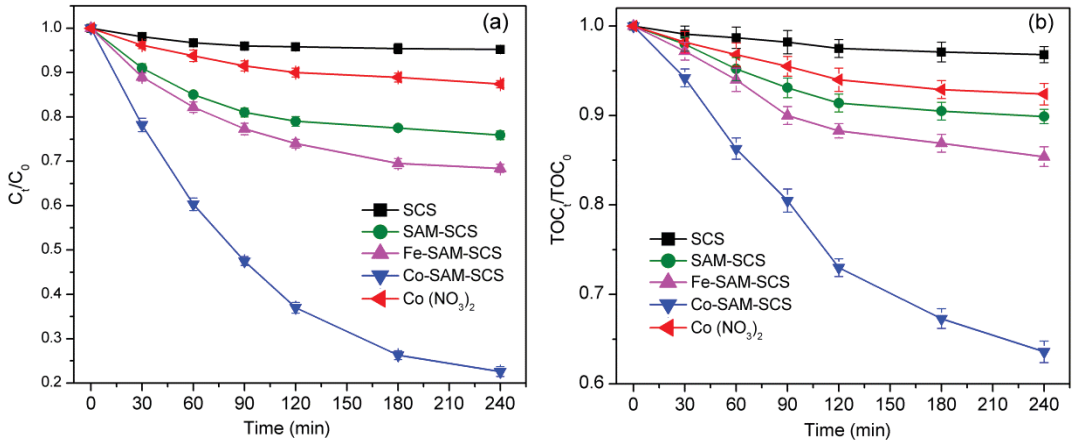

791

792 Fig. 6. The variation of SMZ concentration (a) and TOC (b) in different operation

793 systems. Experiment condition: H_2O_2 concentration = 2%; catalyst loading = 0.7 g/L;

794 SMZ concentration = 50 mg/L; Temperature = 25 °C; initial pH = 7.

795

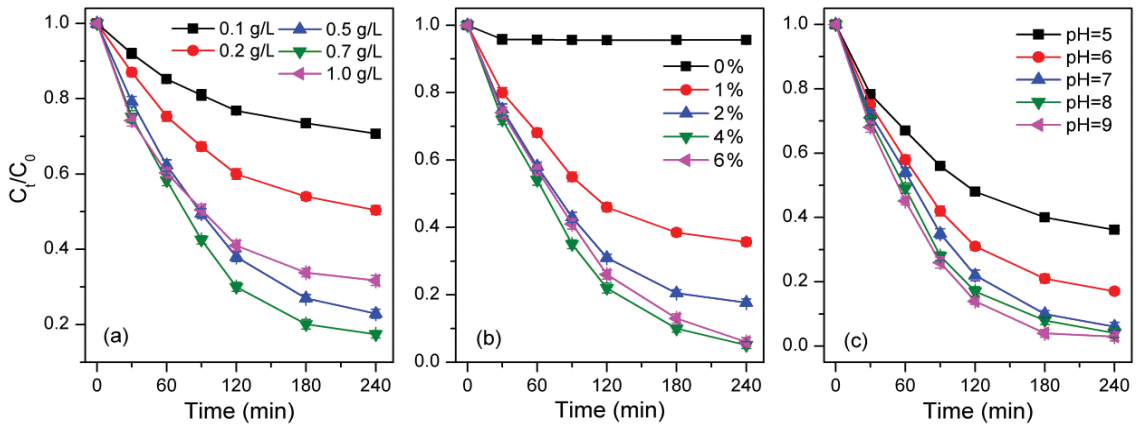

Fig. 7. Effects of (a) catalyst loading, (b) H_2O_2 concentration, and (c) initial pH in degradation rates of SMZ. Experimental conditions: (a) SMZ concentration = 50 mg/L; H_2O_2 concentration = 2%; Temperature = 25 °C; pH = 7; (b) catalyst loading = 0.7 g/L; SMZ concentration = 50 mg/L; Temperature = 25 °C; initial pH = 7; (c) catalyst loading = 0.7 g/L; SMZ concentration = 50 mg/L; H_2O_2 concentration = 4%; Temperature = 25 °C.

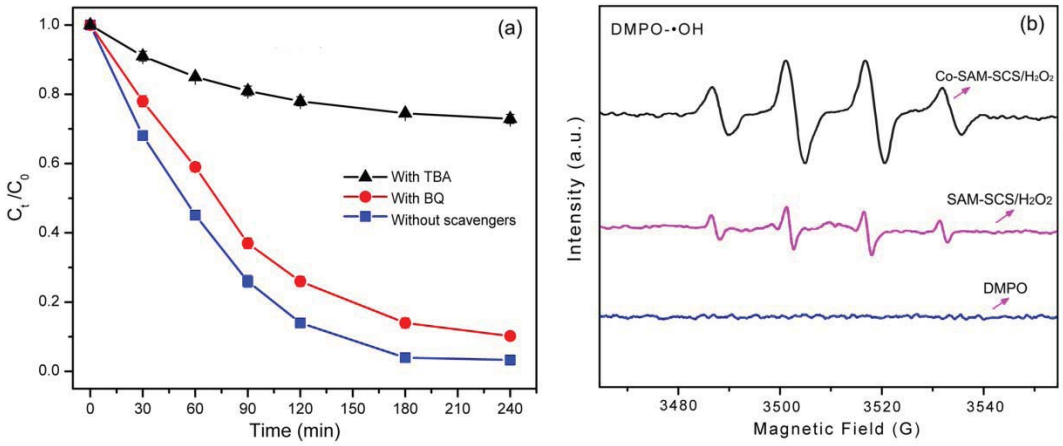

Fig. 8. (a) Effect of radical scavengers on SMZ degradation. Reaction conditions: catalyst loading = 0.7 g/L; H_2O_2 concentration = 4%; Concentration of radical scavenger = 20 mM; Temperature = 25 ◦C; pH= 9. (b) DMPO spin-trapping EPR spectra obtained from different systems. All the spectra were recorded 10 min after mixing. Reaction conditions: catalyst loading = 0.7 g/L; H_2O_2 concentration = 4%; DMPO concentration = 50 mM; Temperature = 25 °C; pH=9.0.

816

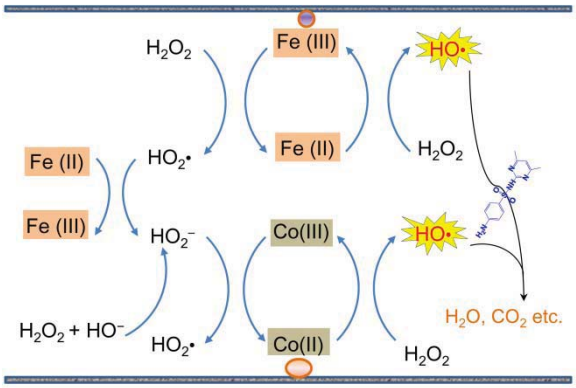

817

818 Fig. 9. Possible activation mechanisms of H_2O_2 in Co-SAM-SCS/H_2O_2 system.

819

820

821

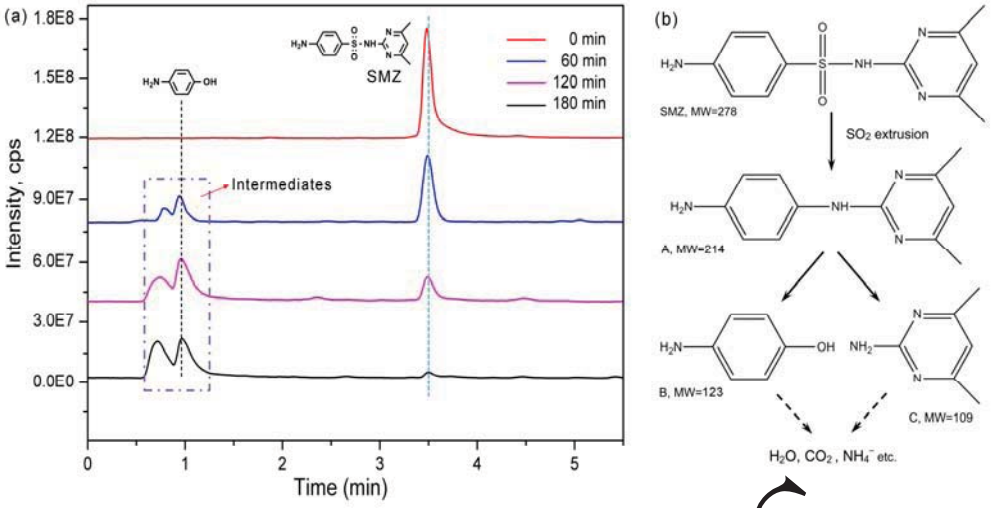

822

823 Fig. 10. LC spectra of the intermediates detected in the Co-SAM-SCS/H_2O_2 system

824 (a.), and the proposed degradation pathways of SMZ in this system (b).

825

826

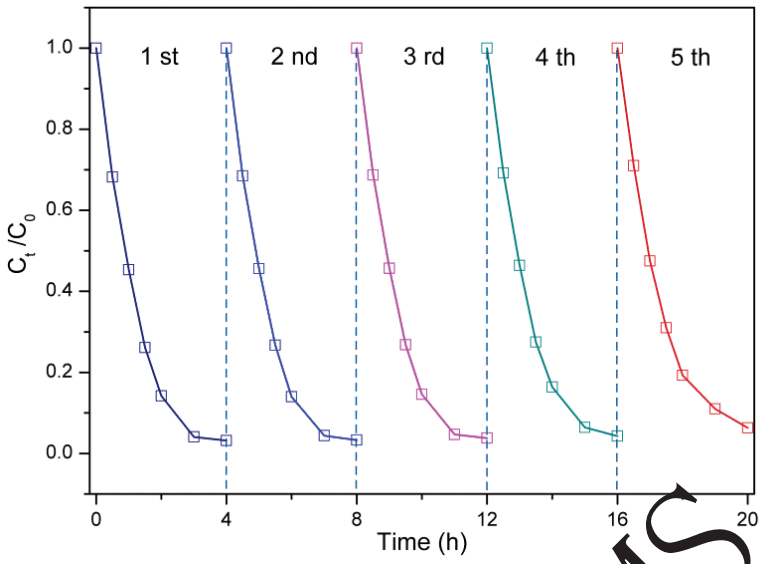

827

828 Fig. 11. Cycling runs for the degradation of SMZ in the presence of Co-SAM-SCS

829 and H_2O_2. Experimental conditions: catalyst loading = 0.7 g/L; SMZ concentration =

830 50 mg/L; H_2O_2 concentration = 4%; Temperature = 25 °C.

831

832

833

834 Table 1 Summary of the treatment costs of different AOPs. The total treatment cost includes the energy and chemical costs.

Process	Pollutants and the concentrations	Chemicals and the concentrations	Operating conditions	Removal efficiency	Total treatment cost	Reference
Hydrodynamic cavitation + O_3 + H_2O_2	Carbamazepine: 10 mg/L	O_3 flow rate: 400 mg/h H_2O_2: 50 mg/L	Volume: 4 L; pH: 4; inlet pressure: 5 bar	100%	4.55 US$/m^3	Thanekar et al. 2018
O_3 + sonication	Dichlorvos: 20 mg/L	O_3 flow rate: 576 mg/h	Volume: 7 L; pH: 3; ultrasonic: 36 kHz	100%	9.1 US$/m^3	Patil and Gogate 2015
TiO_2 + solar	Dichlorvos: 20 mg/L	TiO_2: 100 mg/L	Volume: 7 L; pH: 3	78.4%	4.23 US$/m^3	Patil and Gogate, 2015
Fenton-like + sonication	Reactive black 5: 49.6 mg/L	Fe(0): 1000 mg/L H_2O_2: 350 mg/L	Volume: 1 L; pH: 3; ultrasonic: 60 kHz	99%	2.25 US$/m^3	Weng et al. 2013
Fenton-like + sonication	Reactive orange 107: 50 mg/L	Fe_3O_4: 800 mg/L H_2O_2: 340 mg/L	Volume: 0.7 L; pH: 3; ultrasonic: 24 kHz	100%	13.07 US$/m^3	Jaafarzadeh et al. 2018
Fenton-like	Sulfamethazine: 50 mg/L	Co-SAM-SCS: 700 mg/L H_2O_2: 12 g/L	Volume: 0.1 L; pH: 9	96.7%	10.0 US$/m^3	This study

835